arXiv:1704.02564v2 [physics.bio-ph] 27 Apr 2017

Multi-dimensional Cellular Information Processing of Dynamical Patterns

Yoshihiko Hasegawa*
Department of Information and Communication Engineering,
Graduate School of Information Science and Technology,
The University of Tokyo, Tokyo 113-8656, Japan
(Dated: April 28, 2017)

Cells receive signaling molecules by receptors and relay the information via sensory networks so that they can respond properly depending on the type of signals. Recent studies show that cells can extract multi-dimensional information from dynamical concentration patterns of signaling molecules. Here we study how cells generally and optimally process multi-dimensional information embedded in dynamical patterns through biochemical networks. Considering a deterministic limit, we model the decoding networks by linear response functions, and optimize the functions with the calculus of variations to maximize the mutual information between patterns and output. We find that optimal decoders are realized with multiple distinct non-monotonic response functions and that such optimal decoders can extract information much more efficiently than typical single-layer linear decoders. We also consider the decorrelation of information embedded in the dynamical patterns and show that decorrelating decoders converge to the upper bound of the mutual information in the weak noise limit. We explore the biochemical implementations of these decoders using control theory and demonstrate that they can be implemented biochemically through modification of cascade-type networks, which are prevalent in actual signaling pathways.

Introduction.—Cells receive signals by receptors and subsequently process the obtained information through biochemical networks so that they can respond properly. In addition to static information such as concentration or identity of signaling molecules, recent experimental evidence shows that cells can process dynamical patterns [1–6]. Specifically, it was reported that biochemical networks can filter dynamical signals in order to counteract noise or for prediction [7–9]. When processing static information, one molecular species only provides one-dimensional information. On the other hand, dynamical patterns have multi-dimensional information and hence their extraction lets cells learn more about the environment. For multicellular organisms, dynamical patterns are used for inter-cellular communication. It was experimentally reported that multiple messages are embedded in dynamical patterns and each specific pattern is selectively decoded by their downstream molecular networks [6]. One notable advantage of using dynamical patterns for communications over static ones is an ability to encode more information into a common molecular species [10]. Although cellular dynamical information processing has been attracting much attention [7–9, 11–16], very little attention has been paid to multi-dimensional aspects of the information processing of dynamical patterns [10, 17, 18]. Here we study how cells generally and optimally extract multi-dimensional information from dynamical patterns and investigate a biochemical implementation of the optimal decoders. Considering the deterministic limit of decoders, we can describe their response by linear response functions. We obtain an optimal linear response function through the calculus of variations in order to maximize mutual information between dynamical patterns and output. We find that maximal extraction of information is possible with multiple decoders with distinct non-monotonic linear response functions and that such optimal decoders can read out more information from dynamical patterns than single-layer linear decoders. Furthermore, we consider the decorrelation of information embedded in dynamical patterns and calculate its efficiency. We show that the efficiency, which ranges from 0 to 1 (higher is better), converges to 1 in the weak noise limit. Using control theory, we also show that these optimal decoders can be implemented biochemically by a cascade-type linear signaling network with additional feedforward and feedback loops, which are prevalent in actual signaling pathways.

Models.—We consider a cellular sensory system that reads out extracellular dynamical patterns by receptors, subsequently processes the signal via decoding networks, and finally reports the result as the concentration of output molecular species [Figs. 1(a) and (b)]. We assume that there exist N decoding systems, each of which consists of a receptor and subsequent decoding network [$N = 2$ for Figs. 1(a) and (b)]. Multiple decoding systems may belong to the same cell (Fig. 1(a)) or to different cells (Fig. 1(b)), but our model equation does not depend on whether decoding systems belong to the same cell. As each dynamical pattern has infinite dimension, a definition of their probability density function is not trivial. We model a dynamical pattern $w(t)$ by a sum of basis functions after Ref. [19]: $w(t) = \sum_{i=1}^{M} v_i \eta_i(t)$, where M is the number of bases, $\boldsymbol{\eta}(t) = (\eta_1(t), ..., \eta_M(t))$ are basis functions, and $\boldsymbol{v} = (v_1, ..., v_M)$ are their coefficients. The basis functions need not be orthogonal but we demand that $\boldsymbol{\eta}(t)$ be linearly independent. We define probability density $P(\boldsymbol{v})$ on $\boldsymbol{v}$, which are used to define the probability density of the dynamical patterns.

We assume that $\eta_i(t)$ is in a steady state for $t < 0$,

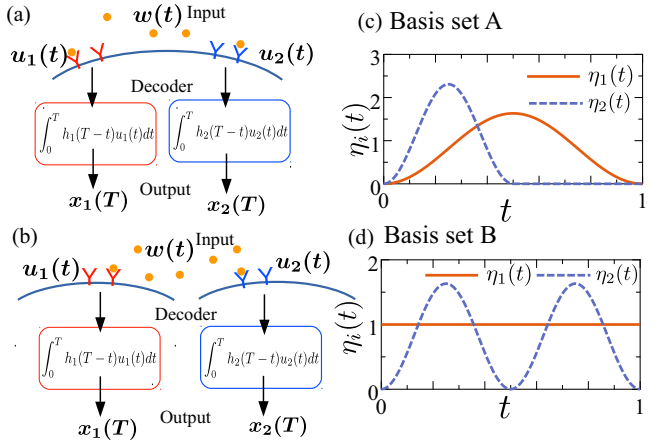

FIG. 1: (Color online) (a) and (b) Decoding of dynamical patterns by two decoding systems. Input signal $w(t)$ is received by N receptors and the signal is processed by subsequent internal molecular decoders [in (a) or (b), decoding networks belong to the same cell or to different cells, respectively]. The linear response function of the ith decoder is given by $h_i(t)$. Each decoder outputs results by $x_i(T)$. (c) and (d) Basis sets for the $M = 2$ case [solid and dashed lines denote $\eta_1(t)$ and $\eta_2(t)$, respectively]. (c) Slow and fast patterns (basis set A). (d) Constant and oscillation patterns (basis set B).

where we define $\eta_i(t) = 0$ for the steady state concentration (and hence $w(t) = 0$ for $t < 0$), and $w(t)$ starts to change at time $t = 0$. Due to stochasticity accompanied with, e.g., stochastic receptor-ligand binding, each decoder reads out a degraded pattern $u_i(t)$: $u_i(t) = w(t) + \xi_i(t)$, where $\xi_i(t)$ is the input noise of the ith receptor defined by $\langle \xi_i(t) \rangle = 0$, and $\langle \xi_i(t)\xi_j(t') \rangle = 2D_i\delta_{ij}\delta(t-t')$, where D_i is the noise intensity. Let $x_i(t)$ be the output concentration of the ith decoder at time t and, for $t < 0$, define $x_i(0) = 0$. Note that $w(t)$ and $x_i(t)$ are concentrations relative to steady state, and thus they can take negative values. We assume that decoders output results after a finite time $t = T$ (for simplicity, we set the same time interval for each decoder) and thus $\boldsymbol{x}(T) = (x_1(T), ..., x_N(T))$ contain information on the dynamical pattern. The amount of information contained in the output is quantified by the mutual information $I[\boldsymbol{x}; \boldsymbol{v}] = \int d\boldsymbol{x} \int d\boldsymbol{v}\, P(\boldsymbol{x}|\boldsymbol{v})P(\boldsymbol{v}) \ln [P(\boldsymbol{x}|\boldsymbol{v})/P(\boldsymbol{x})]$, which is the quantity defined between $\boldsymbol{x}$ and $\boldsymbol{v}$ at time $t = T$. Here $P(\boldsymbol{x}|\boldsymbol{v})$ is the probability density of $\boldsymbol{x}$ given $\boldsymbol{v}$ at time $t = T$, $P(\boldsymbol{v})$ is the probability density on $\boldsymbol{v} = (v_1, .., v_M)$. We assume independent probability density $P(\boldsymbol{v}) = \prod_{i=1}^{M} P(v_i)$ for v_i, where $P(v_i)$ is the Gaussian distribution with mean 0 and variance $\sigma_{v_i}^2$. In our model, we can show that $I[\boldsymbol{x}; \boldsymbol{v}] = \sum_{i=1}^{N} I[x_i; \boldsymbol{v}] - C[\boldsymbol{x}]$, where $C[\boldsymbol{x}] = \int d\boldsymbol{x}\, P(\boldsymbol{x}) \ln \left[P(\boldsymbol{x}) / \prod_{i=1}^{N} P(x_i) \right]$ is the multiinformation (or the total correlation) among $\boldsymbol{x}$ [20, 21], which is a multivariate generalization of the mutual information.

We next model the dynamics of the decoders. To make analytic calculation possible, we consider a deterministic limit of decoders [9, 22] (which corresponds to vanishing intrinsic noise). Suppose that the ith decoder is a single layer linear decoder (push-pull) given by $\dot{z}_i(t) = -\theta_i z_i + u_i(t)$, where $z_i(t)$ is the concentration of molecular species in the decoder and θ_i is the degradation rate. In this decoder, $z_i(t)$ directly reports the result, i.e., $x_i(T) = z_i(T)$. A similar model was proposed for decoding calcium oscillation [23]. The output at time t is given by a convolution integral: $x_i(t) = \int_0^t h_i(t-t')u_i(t')dt'$, where $h_i(t)$ is the linear response function. For this single-layer and linear case, $h_i(t) = e^{-\theta_i t}$. For arbitrary linear response functions, the average at $t = T$ is $\mu_{x_i} = \langle x_i(T) \rangle = \int_0^T h_i(T-t')w(t')dt'$ and the variance is $\sigma_{x_i}^2 = \int_0^T h_i(t')^2 dt'$ [19] (see supplementary material). Biochemical decoders are often composed of multiple layers, which can yield complex linear response functions $h_i(t)$ [cf. Eq. (2)] [8, 9, 22]. We wish to find optimal decoders which maximally extract information from dynamical patterns. Instead of exploring all possible candidate structures, we optimize a set of linear response functions $\boldsymbol{h}(t) = (h_1(t), ..., h_N(t))$ with the calculus of variations. Considering optimization problems in biological systems has two important advantages [24–26]. First, biological systems are considered to be optimal so that they can function efficiently in their environments. Therefore, it might be possible to account for existing biological systems as the optimal solutions for identifiable objectives. Second, optimal decoders provide upper bounds on performance.

Taking into account biological situations, we consider the following three optimization problems (italicized words in parentheses are abbreviations): (i) maximization of $I[\boldsymbol{x}; \boldsymbol{v}]$ (*full decoder*), (ii) maximization of $I[\boldsymbol{x}; \boldsymbol{v}]$ with $C[\boldsymbol{x}] = 0$ (*decorrelating decoder*), and (iii) maximization of $I[\boldsymbol{x}; \boldsymbol{v}]$ with single-layer linear decoders (*SLL decoder*). For (i), decoders obtained by full maximization provide an upper bound on the mutual information between dynamical patterns and output. When cells want to extract as much information as possible, this maximization is suitable. For (ii), when $C[\boldsymbol{x}] = 0$ is satisfied, output $\boldsymbol{x}$ is decorrelated. This condition can be easily incorporated into the maximization if $N = M$, which is assumed here. As the input noises $\boldsymbol{\xi}(t)$ affect each receptor independently (Figs. 1(a) and (b)), we have $P(\boldsymbol{x}|\boldsymbol{v}) = \prod_{i=1}^{N} P(x_i|\boldsymbol{v})$. Combining these relations, we arrive at $P(\boldsymbol{x}) = \int d\boldsymbol{v}\, P(\boldsymbol{x}|\boldsymbol{v})P(\boldsymbol{v}) = \int d\boldsymbol{v} \prod_{i=1}^{N} P(x_i|\boldsymbol{v}) \prod_{j=1}^{N} P(v_j)$. If each $P(x_i|\boldsymbol{v})$ disjointly depends on only one v_i [i.e., $P(x_i|\boldsymbol{v}) = P(x_i|v_i)$], we can show that $P(\boldsymbol{x}) = \prod_i P(x_i)$. This is similar to a decorrelator in digital communication, which decorrelates multiplexed signals (see supplementary material). When different cells receive dynamical patterns as in Fig. 1(b), decorrelated information is desired because information

of each v_i can be obtained by measuring only one $x_i(T)$. Under the constraint $C[\boldsymbol{x}] = 0$, maximization of $I[\boldsymbol{x};\boldsymbol{v}]$ is equivalent to maximization of $\sum_{i=1}^{N} I[x_i;\boldsymbol{v}]$. For (iii), we fix the linear response function to $h_i(t) = e^{-\theta_i t}$, which corresponds to the abovementioned single-layer linear (SLL) decoder. We optimize all θ_i numerically with simulated annealing to maximize $I[\boldsymbol{x};\boldsymbol{v}]$.

For arbitrary N and M (full and decorrelating), we obtain the optimal linear response functions as follows (see supplementary material):

$$h_i(t) = -\frac{\sum_j \lambda_{ij}}{4\Lambda_i D_i}\eta_j(T-t), \tag{1}$$

where λ_{ij} and Λ_i are Lagrange multipliers (real values) and these values depend on the type of decoders (full or decorrelating).

Results.—We construct concrete optimal linear response functions for a system with $N = M = 2$ and $T = 1$. For the basis functions $\eta_i(t)$, we consider the two basis sets shown in Figs. 1(c) and (d): basis set A comprising slow $\eta_1(t) = \sqrt{2/3}(1-\cos(2\pi t))$ and fast $\eta_2(t) = (2/\sqrt{3})\Theta(1/2-t)(1-\cos(4\pi t))$ patterns (Fig. 1(c)), where $\Theta(t)$ is a step function, and basis set B comprising constant $\eta_1(t) = 1$ and oscillation $\eta_2(t) = \sqrt{2/3}(1-\cos(4\pi t))$ patterns (Fig. 1(d)). All the bases are normalized so that $\int_0^T \eta_i(t)^2 dt = 1$.

Let $I^{\rm full}$, $I^{\rm decor}$, and $I^{\rm sll}$ be the mutual information $I[\boldsymbol{x};\boldsymbol{v}]$ of the full, decorrelating, and SLL decoders, respectively. Figures 2(a) and (b) show the three mutual informations as functions of the noise intensity $D(= D_1 = D_2)$ for the basis sets A and B, respectively. In these figures, solid, dashed, and dotted lines denote $I^{\rm full}$,$I^{\rm decor}$, and $I^{\rm sll}$, respectively, and parameter details are shown in the caption of Fig. 2. In the figures, we see that $I^{\rm full}$ and $I^{\rm decor}$ yield higher values than $I^{\rm sll}$ for a lower noise intensity D, especially in Fig. 2(a), which indicates that non-monotonic response functions extract information more efficiently than SLL decoders. For a lower noise intensity D, the mutual information difference $\Delta I = I^{\rm full} - I^{\rm decor}$ is near constant and smaller for basis set A (Fig. 2(a)) than for basis set B (Fig. 2(b)). In order to account for these differences, we introduce the correlation matrix $\{\psi_{ij}\}$ of the bases $\eta_i(t)$: $\psi_{ij} = \int_0^T \eta_i(t)\eta_j(t)dt$. For $D \ll 1$, we find that the mutual information difference is $\Delta I = I^{\rm full} - I^{\rm decor} \simeq -(1/2)\ln\left(1 - \psi_{12}^2/(\psi_{11}\psi_{22})\right)$ and hence a smaller cross-correlation ψ_{12} yields a smaller difference of ΔI ($\Delta I = 0.13$ for basis set A and $\Delta I = 0.55$ for basis set B). We define the efficiency $\mathcal{E}$ ($0 \le \mathcal{E} \le 1$) for the decorrelating and SLL decoders by $\mathcal{E}^{\rm decor} = I^{\rm decor}/I^{\rm full}$ and $\mathcal{E}^{\rm sll} = I^{\rm sll}/I^{\rm full}$, which are shown in Figs. 2(c) and (d) for the basis sets A and B, respectively. For the both basis sets, we see that $\mathcal{E}^{\rm decor}$ converges to 1 for decreasing D, indicating that the decorrelating decoder can achieve near optimal efficiency in the weak noise limit.

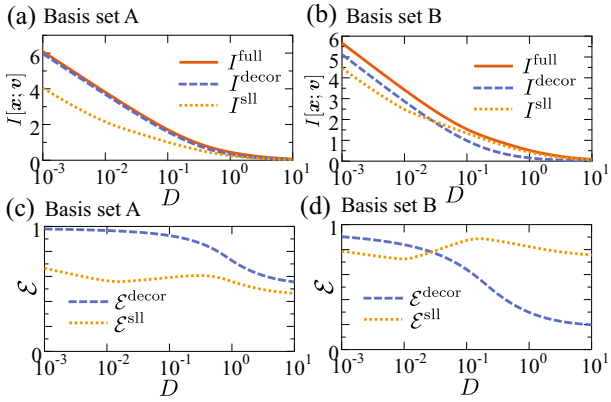

FIG. 2: (Color online) (a) and (b) Mutual information $I[\boldsymbol{x};\boldsymbol{v}]$ as a function of noise intensity D by basis set; (a) basis set A [Fig. 1(c)] and (b) basis set B [Fig. 1(d)]. Solid, dashed, and dotted lines denote $I^{\rm full}$, $I^{\rm decor}$, and $I^{\rm sll}$, respectively. (c) and (d) Efficiency $\mathcal{E}$ as a function of D by basis set; (c) basis set A and (d) basis set B. Dashed and dotted lines denote $\mathcal{E}^{\rm decor}$ and $\mathcal{E}^{\rm sll}$, respectively. Parameters are $T = 1$ and $\sigma_{v_1}^2 = \sigma_{v_2}^2 = 1$.

From Figs. 2(a) and (b), there exists a qualitative behavioral difference between the regions of $D \lesssim 0.1$ (nearly straight line) and $D \gtrsim 0.1$ (curved line) for $I^{\rm full}$ and $I^{\rm decor}$. In order to discover the origin of this difference, we examine the optimal response functions in these regions, which are shown in Fig. 3. Figures 3(a)–(c) show linear response function $h_i(t)$ for the full decoder with basis set A for different noise intensities ($D = 0.1$, 0.5, and 1.0) while keeping the other parameters unchanged (details are shown in the caption of Fig. 3). Note that for $D < 0.1$, the shapes of the optimal linear response functions are similar to that of $D = 0.1$, and for $D > 1.0$, they are similar to that of $D = 1.0$. In Fig. 3(d), we also show the optimal linear response function for the decorrelating decoder. In this case, there is no major difference when noise intensity D is varied. We can see that for $D = 0.1$ (Fig. 3(a)), the linear response function of the full decoder is similar to that of the decorrelating decoder of Fig. 3(d), indicating that the decorrelation can provide near optimal efficiency for the weak noise case. $h_i(t)$ shown by solid and dashed lines mainly decode information embedded in slow and fast patterns, respectively. When we increase D in the full optimal case, the two linear response functions coalesce to a single function (the critical point is $D \simeq 0.83$ for basis set A and $D \simeq 0.20$ for basis set B). This result shows that, when the noise intensity is very high, separate decoding of information embedded in different basis functions is very inefficient, and joint decoding provides more information.

We next explore a biochemical implementation of the optimal decoders. We try to implement a decoding network corresponding to $h_i(t)$ with K_i molecular species (K_i is determined by the degree of the transfer function; see below). Linearizing around the steady state when

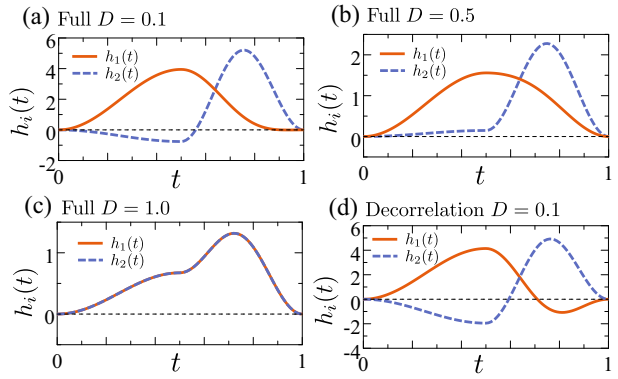

FIG. 3: (Color online) (a)–(c) Optimal linear response function $h_i(t)$ of the full decoder with basis set A for different noise intensities; (a) $D = 0.1$, (b) $D = 0.5$, and (c) $D = 1.0$, where all other parameters are the same. (d) Optimal linear response function $h_i(t)$ of the decorrelating decoder with $D = 0.1$. In (a)–(d), solid and dashed lines denote $h_1(t)$ and $h_2(t)$, respectively. For all $h_i(t)$ shown in (a)–(d), those which are horizontally symmetric with respect to $h_i = 0$ are also optimal solutions. We set $\sigma_{x_1}^2 = \sigma_{x_2}^2 = 1$ and those parameters only affect the magnitude of the functions. Other parameters are identical to those in Fig. 2.

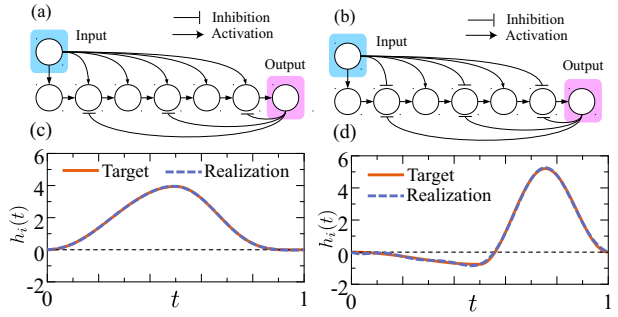

FIG. 4: (Color online) (a) and (b) Molecular realization of the two linear response functions in Fig. 3(a). (a) and (b) correspond to $h_1(t)$ and $h_2(t)$ in Fig. 3(a), respectively. Arrow and bar-headed lines denote activation and inhibition, respectively. (c) and (d) Linear response functions of the realization networks; dashed lines in (c) and (d) are the linear response functions of molecular networks in (a) and (b), respectively. Solid lines denote the target optimal linear response functions shown in Fig. 3(a).

$\langle u_i(t)\rangle = w(t) = 0$, their dynamics are described by the following linear model:

$$\dot{\boldsymbol{z}}_i(t) = \boldsymbol{A}_i \boldsymbol{z}_i(t) + \boldsymbol{b}_i u_i(t). \tag{2}$$

where $\boldsymbol{z}_i(t) = (z_{i1}(t), ..., z_{iK_i}(t))^\top$, $z_{ik}(t)$ is the concentration of the kth molecular species in the ith decoder, $\boldsymbol{A}_i$ is a $K_i \times K_i$ matrix, and $\boldsymbol{b}_i$ is a K_i-dimensional column vector. Output of Eq. (2) is $z_{iK_i}(t)$ and hence $x_i(T) = z_{iK_i}(T)$ (the last molecular species reports the result). Independent of the type of maximization (the full or decorrelating decoders), from Eq. (1), Laplace transform yields $\tilde{h}_i(s) = -1/(4\Lambda_i D_i)\sum_j \lambda_{ij}\tilde{\eta}_j(s)$, where $\tilde{h}_i(s) = \mathcal{L}[h_i(t)]$ (the transfer function) and $\tilde{\eta}_i(s) = \mathcal{L}[\tilde{\eta}_i(T-t)]$ with $\mathcal{L}$ being the Laplace transform. We want to identify $\boldsymbol{A}_i$ and $\boldsymbol{b}_i$ which yield the desired transfer functions $\tilde{h}_i(s)$. This problem is known as the realization problem in control theory [27]. Let the transfer function be a rational polynomial function of the form $\tilde{h}_i(s) = \sum_{k=1}^{K_i}\beta_{ik}s^{K_i-k}/\left\{s^{K_i} + \sum_{k=1}^{K_i}\alpha_{ik}s^{K_i-k}\right\}$ (β_{ik} and α_{ik} are real values), where the degree of the denominator is larger than that of the nominator (this condition is called *strictly proper*). From control theory, one possible realization of this transfer function is (see supplementary material)

$$\boldsymbol{A}_i = \begin{bmatrix} 0 & 0 & 0 & \cdots & -\alpha_{iK_i} \\ 1 & 0 & 0 & \cdots & -\alpha_{i,K_i-1} \\ 0 & 1 & 0 & \cdots & -\alpha_{i,K_i-2} \\ \vdots & \vdots & \vdots & \ddots & \vdots \\ 0 & 0 & 0 & 1 & -\alpha_{i1} \end{bmatrix}, \boldsymbol{b}_i = \begin{bmatrix} \beta_{iK_i} \\ \beta_{i,K_i-1} \\ \beta_{i,K_i-2} \\ \vdots \\ \beta_{i1} \end{bmatrix}. \tag{3}$$

Off-diagonal ones in Eq. (3) imply that z_{ji} depends on $z_{j,i-1}$ $(i = 2, 3, ..., K_j)$, which corresponds to a cascade topology. Surprisingly, when the transfer function is strictly proper, its corresponding linear systems can be implemented by a cascade network with additional feedback and feedforward loops. As is well known, the cascade topology is prevalent in actual signaling networks and additional feedback and feedforward loops exists there, implying that it is possible to implement optimal decoders biochemically. As an example, we construct biochemical implementations of the full decoders for the basis set A with $D = 0.1$ (Fig. 3(a)). We show the biochemical networks in Figs. 4(a) and (b), and their corresponding linear response functions in Figs. 4(c) and (d), respectively. The realization networks are created by applying the Fourier series expansion to $\eta_i(t)$ and calculating their Laplace transform (see supplementary material). In Figs. 4(a) and (b), when matrix elements of $\boldsymbol{A}_i$ and $\boldsymbol{b}_i$ are positive or negative, we display their relation by activation (arrow) or inhibition (bar-headed line), respectively. In Figs. 4(c) and (d), we can see that the linear response functions of the molecular networks (dashed line) are indistinguishable from the target optimal linear response function $h_i(t)$ (solid line). This fact indicates that the biochemical networks which maximally exploit information from dynamical patterns can be implemented. The network in Fig. 4(b) decodes the fast pattern, while that in Fig. 4(a) does the slow one. The main difference between these two networks is that the later has an incoherent feed-forward loop (iFFL) [28, 29], while the former does not. Reference [30] indicated that, when decoding temporal insulin patterns, a decoding network having an iFFL is responsive against a fast pulsatile pattern, while it does not respond to a slow ramp pattern. In the present Letter, both of the implementations have 7 nodes (i.e., $K_i = 7$). However, we note that the molecular networks can be minimized without much los-

ing their response. Indeed, a simple oscillatory linear response similar to $\eta_1(t)$ of basis set A can be implemented by only two nodes.

In this Letter, we considered the mutual information between patterns and output. Recently, extensive efforts have been paid to constructing relations between thermodynamic cost and mutual information [31], especially in biological contexts [32, 33]. Our model considers the deterministic limit and hence it ignores the intrinsic thermal noise. When we incorporate the effect of intrinsic noise, then the mutual information between patterns and output should be upper bounded by some thermodynamic cost. Exploration of this topic is left for future studies.

* Corresponding author : hasegawa.yoshihiko@mail.u-tokyo.ac.jp

[1] M. Behar and A. Hoffmann, Curr. Opin. Genetics Dev. **20**, 684 (2010).
[2] H. Kubota, R. Noguchi, Y. Toyoshima, Y.-i. Ozaki, S. Uda, K. Watanabe, W. Ogawa, and S. Kuroda, Mol. Cell **46**, 820 (2012).
[3] J. E. Purvis and G. Lahav, Mol. Cell **46**, 715 (2012).
[4] M. Behar, D. Barken, S. L. Werner, and A. Hoffmann, Cell **155**, 448 (2013).
[5] J. E. Purvis and G. Lahav, Cell **152**, 945 (2013).
[6] T. Sano, K. Kawata, S. Ohno, K. Yugi, H. Kakuda, H. Kubota, S. Uda, M. Fujii, K. Kunida, D. Hoshino, et al., Sci. Signal. **9**, ra112 (2016).
[7] T. J. Kobayashi, Phys. Rev. Lett. **104**, 228104 (2010).
[8] M. Hinczewski and D. Thirumalai, Phys. Rev. X **4**, 041017 (2014).
[9] N. B. Becker, A. Mugler, and P. R. ten Wolde, Phys. Rev. Lett. **115**, 258103 (2015).
[10] J. Selimkhanov, B. Taylor, J. Yao, A. Pilko, J. Albeck, A. Hoffmann, L. Tsimring, and R. Wollman, Science **346**, 1370 (2014).
[11] F. Tostevin and P. R. ten Wolde, Phys. Rev. Lett. **102**, 218101 (2009).
[12] T. Mora and N. S. Wingreen, Phys. Rev. Lett. **104**, 248101 (2010).
[13] A. Mugler, A. M. Walczak, and C. H. Wiggins, Phys. Rev. Lett. **105**, 058101 (2010).
[14] A. S. Hansen and E. K. O'Shea, Mol. Syst. Biol. **9**, 704 (2013).
[15] S. S. Mc Mahon, O. Lenive, S. Filippi, and M. P. H. Stumpf, J. R. Soc. Interface **12**, 20150597 (2015).
[16] H. K. Makadia, J. S. Schwaber, and R. Vadigepalli, PLoS Comput. Biol. **11**, e1004563 (2015).
[17] W. de Ronde, F. Tostevin, and P. R. ten Wolde, Phys. Rev. Lett. **107**, 048101 (2011).
[18] W. de Ronde and P. R. ten Wolde, Phys. Biol. **11**, 026004 (2014).
[19] R. G. Gallager, *Information theory and reliable communication*, vol. 2 (Springer, 1968).
[20] S. Watanabe, IBM Journal of research and development **4**, 66 (1960).
[21] M. Studenỳ and J. Vejnarová, in *Learning in graphical models* (Springer, 1998), pp. 261–297.
[22] C. C. Govern and P. R. ten Wolde, Phys. Rev. Lett. **109**, 218103 (2012).
[23] M. Marhl, M. Perc, and S. Schuster, Biophys. Chem. **120**, 161 (2006).
[24] Y. Hasegawa and M. Arita, J. R. Soc. Interface **11**, 20131018 (2014).
[25] Y. Hasegawa and M. Arita, Phys. Rev. Lett. **113**, 108101 (2014).
[26] Y. Hasegawa, New J. Phys. **18**, 113031 (2016).
[27] R. L. Williams and D. A. Lawrence, *Linear state-space control systems* (John Wiley & Sons, 2007).
[28] S. Mangan and U. Alon, Proc. Natl. Acad. Sci. U.S.A. **100**, 11980 (2003).
[29] U. Alon, *An Introduction to Systems Biology* (CRC Press, 2007).
[30] R. Noguchi, H. Kubota, K. Yugi, Y. Toyoshima, Y. Komori, T. Soga, and S. Kuroda, Mol. Syst. Biol. **9**, 664 (2013).
[31] J. M. R. Parrondo, J. M. Horowitz, and T. Sagawa, Nat. Phys. **11**, 131 (2015).
[32] P. Sartori, L. Granger, C. F. Lee, and J. M. Horowitz, PLoS Comput. Biol. **10**, e1003974 (2014).
[33] A. C. Barato, D. Hartich, and U. Seifert, New J. Phys. **16**, 103024 (2014).

arXiv:1704.02564v2 [physics.bio-ph] 27 Apr 2017

Supplementary Material for "Multi-dimensional Cellular Information Processing of Dynamical Patterns"

Yoshihiko Hasegawa

This supplementary material describes in detail the calculations introduced in the main text. Equation and figure numbers in this section are prefixed with S (e.g., Eq. (S1) or Fig. S1). Numbers without the prefix (e.g., Eq. (1)or Fig. 1) refer to items in the main text.

1 Mean and variance of output

We calculate the mean and the variance of output of the ith decoder as follows. We define $w(t)$ as an input signal which is the sum of basis functions $\eta_i(t)$ with weights v_i: $w(t) = \sum_{i=1}^{M} v_i \eta_i(t)$. As described in the main text, we can express the output of the ith decoder by

$$x_i(t) = \int_0^t h_i(t-t')u_i(t')dt', \tag{S1}$$

where $h_i(t)$ is a linear response function and $u_i(t) = w(t) + \xi_i(t)$ [$\xi_i(t)$ is white Gaussian noise with the correlation $\langle \xi_i(t)\xi_j(t)\rangle = 2D_i\delta_{ij}\delta(t-t')$ in which D_i is the noise intensity]. The mean at time $t = T$ is

$$\mu_{x_i} = \langle x_i(T)\rangle = \int_0^T h_i(T-t')\left\langle w(t') + \xi_i(t')\right\rangle dt' = \int_0^T h_i(T-t')w(t')dt' = \sum_{j=1}^{M} v_j q_{ij}, \tag{S2}$$

where we define

$$q_{ij} = \int_0^T h_i(T-t')\eta_j(t')dt'. \tag{S3}$$

Similarly, the variance at time $t = T$ is given by

$$\begin{aligned}
\sigma_{x_i}^2 &= \left\langle x_i(T)^2\right\rangle - \left\langle x_i(T)\right\rangle^2, \\
&= \int_0^T dt' \int_0^T dt''\, h_i(T-t')h_i(T-t'')\left\langle \xi_i(t')\xi_i(t'')\right\rangle, \\
&= 2D_i \int_0^T h_i(t')^2 dt'.
\end{aligned} \tag{S4}$$

According to the Gaussian assumption of probability density of x_i, at time $t = T$, we have

$$P(x_i|\boldsymbol{v}) = \frac{1}{\sqrt{2\pi\sigma_{x_i}^2}} \exp\left(-\frac{\left(x_i - \sum_{j=1}^{M} v_j q_{ij}\right)^2}{2\sigma_{x_i}^2}\right). \tag{S5}$$

As assumed in the main text, the probability distribution of v_i is given by

$$P(v_i) = \frac{1}{\sqrt{2\pi\sigma_{v_i}^2}} \exp\left(-\frac{v_i^2}{2\sigma_{v_i}^2}\right). \tag{S6}$$

2 Mutual information

The mutual information $I[\boldsymbol{x};\boldsymbol{v}]$ and multiinformation $C[\boldsymbol{x}]$ are defined by

$$C[\boldsymbol{x}] = \int d\boldsymbol{x}\, P(\boldsymbol{x}) \ln \frac{P(\boldsymbol{x})}{\prod_{i=1}^{N} P(x_i)}, \tag{S7}$$

$$I[\boldsymbol{x};\boldsymbol{v}] = \int d\boldsymbol{x} \int d\boldsymbol{v}\, P(\boldsymbol{x}|\boldsymbol{v}) P(\boldsymbol{v}) \ln \frac{P(\boldsymbol{x}|\boldsymbol{v})}{P(\boldsymbol{x})}. \tag{S8}$$

For $N = M = 2$ which is considered in the Letter, with Eqs. (S5) and (S6), we have the following expressions:

$$C[x_1, x_2] = -\frac{1}{2} \ln \left[1 - \frac{\left(q_{11} q_{21} \sigma_{v_1}^2 + q_{12} q_{22} \sigma_{v_2}^2 \right)^2}{\left(q_{11}^2 \sigma_{v_1}^2 + q_{12}^2 \sigma_{v_2}^2 + \sigma_{x_1}^2 \right) \left(q_{21}^2 \sigma_{v_1}^2 + q_{22}^2 \sigma_{v_2}^2 + \sigma_{x_2}^2 \right)} \right], \tag{S9}$$

$$I[x_1, x_2; v_1, v_2] = \frac{1}{2} \ln \left[1 + \frac{q_{11}^2 \sigma_{v_1}^2 + q_{12}^2 \sigma_{v_2}^2}{\sigma_{x_1}^2} + \frac{q_{21}^2 \sigma_{v_1}^2 + q_{22}^2 \sigma_{v_2}^2}{\sigma_{x_2}^2} + \frac{\sigma_{v_1}^2 \sigma_{v_2}^2 (q_{11} q_{22} - q_{12} q_{21})^2}{\sigma_{x_1}^2 \sigma_{x_2}^2} \right], \tag{S10}$$

$$\begin{aligned} I[x_1, x_2; v_1, v_2] + C[x_1, x_2] &= I[x_1; v_1, v_2] + I[x_2; v_1, v_2], \\ &= \frac{1}{2} \ln \left[\frac{\left(q_{11}^2 \sigma_{v_1}^2 + q_{12}^2 \sigma_{v_2}^2 + \sigma_{x_1}^2 \right) \left(q_{21}^2 \sigma_{v_1}^2 + q_{22}^2 \sigma_{v_2}^2 + \sigma_{x_2}^2 \right)}{\sigma_{x_1}^2 \sigma_{x_2}^2} \right]. \end{aligned} \tag{S11}$$

3 Optimal linear response function

We calculate optimal linear response function $h_i(t)$ which maximizes the mutual information $I[\boldsymbol{x};\boldsymbol{v}]$. As can be seen with Eq. (S10), the mutual information $I[\boldsymbol{x};\boldsymbol{v}]$ is a function of $\boldsymbol{q} = (q_{ij})$. Instead of directly maximizing $I[\boldsymbol{x};\boldsymbol{v}]$, we consider a more tractable function $\mathcal{M}(\boldsymbol{q})$ which satisfies the following condition:

$$\operatorname*{argmax}_{\boldsymbol{q}} I[\boldsymbol{x};\boldsymbol{v}] = \operatorname*{argmax}_{\boldsymbol{q}} \mathcal{M}(\boldsymbol{q}).$$

Then we consider the following performance index $\mathcal{R}(\boldsymbol{q}, \boldsymbol{h})$:

$$\mathcal{R}(\boldsymbol{q}, \boldsymbol{h}) = \mathcal{M}(\boldsymbol{q}) + \sum_{i,j} \lambda_{ij} \left(q_{ij} - \int_0^T h_i(T-t) \eta_j(t) dt \right) + \sum_i \Lambda_i \left(\sigma_{x_i}^2 - 2D_i \int_0^T h_i(t)^2 dt \right), \tag{S12}$$

where λ_{ij} and Λ_i are the Lagrange multipliers. Note that arguments of $\boldsymbol{q}$ in Eq. (S12) are scalars while $\boldsymbol{h}$ are functions. Constraints corresponding to λ_{ij} and Λ_i are derived from Eqs. (S3) and (S4), respectively. Because $I[\boldsymbol{x};\boldsymbol{v}]$ is scale-invariant with respect to $h_i(t)$ and hence σ_{x_i} does not affect the mutual information, we set σ_{x_i} as a constant variable (we set $\sigma_{x_i} = 1$ for all i in the main text). The total derivative of $\mathcal{R}(\boldsymbol{q}, \boldsymbol{h})$ is written by

$$\begin{aligned} d\mathcal{R} &= \sum_{i,j} \frac{\partial \mathcal{M}(\boldsymbol{q})}{\partial q_{ij}} dq_{ij} + \sum_{i,j} \lambda_{ij} \left(dq_{ij} - \int_0^T \delta h_i(t) \eta_j(T-t) dt \right) + \sum_i \Lambda_i \left(-4D_i \int_0^T h_i(t) \delta h_i(t) dt \right), \\ &= \sum_{i,j} \left(\frac{\partial \mathcal{M}(\boldsymbol{q})}{\partial q_{ij}} + \lambda_{ij} \right) dq_{ij} + \sum_i \int_0^T \delta h_i(t) \left(-\sum_j \lambda_{ij} \eta_j(T-t) - 4D_i \Lambda_i h_i(t) \right) dt. \end{aligned} \tag{S13}$$

Because, $d\mathcal{R}$ should vanish at a stationary point for arbitrary dq_{ij} and δh_i, we obtain the following relations:

$$\frac{\partial \mathcal{M}(\boldsymbol{q})}{\partial q_{ij}} + \lambda_{ij} = 0, \tag{S14}$$

$$-\sum_j \lambda_{ij} \eta_j(T-t) - 4D_i \Lambda_i h_i(t) = 0. \tag{S15}$$

From Eq. (S15), we have

$$h_i(t) = -\frac{\sum_j \lambda_{ij} \eta_j(T-t)}{4\Lambda_i D_i}, \tag{S16}$$

which is Eq. (1) in the main text. Depending on the type of decoders (full or decorrelating), λ_{ij} and Λ_i are determined (see below). From Eqs. (S3) and (S4), we further have

$$q_{ij} = -\frac{1}{4\Lambda_i D_i}\sum_k \lambda_{ik}\psi_{kj}, \tag{S17}$$

$$\sigma_{x_i}^2 = \frac{1}{8\Lambda_i^2 D_i}\sum_{j,k}\lambda_{ij}\lambda_{ik}\psi_{kj},, \tag{S18}$$

where $\{\psi_{ij}\}$ is a correlation matrix of the basis functions $\eta_i(t)$, defined by

$$\psi_{ij} = \int_0^T \eta_i(t)\eta_j(t)dt.$$

Algebraic equations (S14), (S17), and (S18) are solved with respect to $\boldsymbol{q}$, $\boldsymbol{\lambda}$, and $\boldsymbol{\Lambda}$ to obtain the maximum of $I[\boldsymbol{x};\boldsymbol{v}]$.

3.1 Full decoder

According to Eq. (S10), we can use the following function for the full decoder:

$$\mathcal{M}(\boldsymbol{q}) = \frac{q_{11}^2\sigma_{v_1}^2 + q_{12}^2\sigma_{v_2}^2}{\sigma_{x_1}^2} + \frac{q_{21}^2\sigma_{v_1}^2 + q_{22}^2\sigma_{v_2}^2}{\sigma_{x_2}^2} + \frac{\sigma_{v_1}^2\sigma_{v_2}^2(q_{11}q_{22}-q_{12}q_{21})^2}{\sigma_{x_1}^2\sigma_{x_2}^2}, \tag{S19}$$

Because it is difficult to obtain closed-form solutions for Eqs. (S14), (S17), and (S18) along with Eq. (S19), we numerically solve the equations.

When the noise intensity D_i is sufficiently weak, we find the following expression:

$$\begin{aligned} I^{\text{full}} &\simeq \frac{1}{2}\ln\left[\frac{\sigma_{v_1}^2\sigma_{v_2}^2(q_{11}q_{22}-q_{12}q_{21})^2}{\sigma_{x_1}^2\sigma_{x_2}^2}\right], \\ &= \frac{1}{2}\ln\left[\frac{\sigma_{v_1}^2\sigma_{v_2}^2\left(\psi_{11}\psi_{22}-\psi_{12}^2\right)}{4D_1D_2}\right]. \end{aligned}$$

3.2 Decorrelating decoder

For $N = M(=2)$, which is considered in the Letter, decorrelation is easily implemented. The output of the ith decoder is denoted by x_i and its probability density is $P(x_i|\boldsymbol{v})$ (Eq. (S5)). The relation can be represented by the Bayesian network shown in Fig. S1(a). For this case, the output probability density is not decorrelated, i.e., $P(\boldsymbol{x}) \neq \prod_i P(x_i)$. When $P(x_i|\boldsymbol{v})$ disjointly depends on only one $v_j \in \boldsymbol{v}$, which is shown in Fig. S1(b) for $P(x_i|v_i)$, the output probability density is decorrelated. We can use the following function for the decorrelating decoder:

$$\mathcal{M}(\boldsymbol{q}) = \frac{q_{11}^2\sigma_{v_1}^2}{\sigma_{x_1}^2} + \frac{q_{22}^2\sigma_{v_2}^2}{\sigma_{x_2}^2} + \frac{\sigma_{v_1}^2\sigma_{v_2}^2 q_{11}^2 q_{22}^2}{\sigma_{x_1}^2\sigma_{x_2}^2}, \tag{S20}$$

where we use $q_{ij} = 0$ $(i \neq j)$. We obtain the mutual information as follows:

$$I^{\text{decor}} = \frac{1}{2}\ln\left[1 + \frac{\left(\psi_{11}\psi_{22}-\psi_{12}^2\right)\left(2D_1\psi_{22}\sigma_{v_2}^2 + 2D_2\psi_{11}\sigma_{v_1}^2 + \left(\psi_{22}\psi_{11}-\psi_{12}^2\right)\sigma_{v_1}^2\sigma_{v_2}^2\right)}{4D_1D_2\psi_{11}\psi_{22}}\right].$$

When the noise intensity D_i is sufficiently weak, the mutual information reduces to the following expression:

$$I^{\text{decor}} \simeq \frac{1}{2}\ln\left[\frac{\sigma_{v_1}^2\sigma_{v_2}^2\left(\psi_{11}\psi_{22}-\psi_{12}^2\right)^2}{4D_1D_2\psi_{11}\psi_{22}}\right].$$

4 Network realization of transfer function

In the main text, we explore biochemical realization of optimal linear response functions $h_i(t)$. We consider a general K-dimensional linear system:

$$\dot{\boldsymbol{z}}(t) = \boldsymbol{A}\boldsymbol{z}(t) + \boldsymbol{b}u(t), \quad y(t) = \boldsymbol{c}\boldsymbol{z}(t), \tag{S21}$$

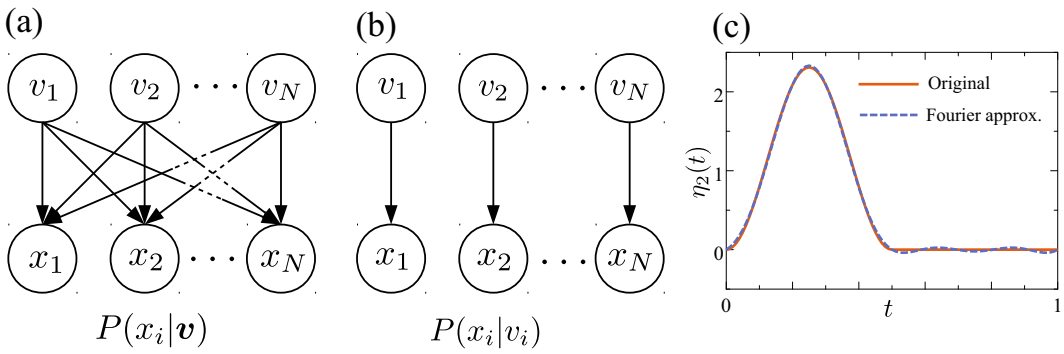

Figure S1: (a) and (b) Network representations of (a) $P(x_i|\boldsymbol{v})$ and (b) $P(x_i|v_i)$ for $N = M$. (c) Basis function $\eta_2(t)$ of basis set A [Fig. 1(c)] (solid line) and its Fourier series approximation (dashed line).

where $\boldsymbol{z}(t)$ is a K-dimensional column vector, $y(t)$ is an output scalar variable, $\boldsymbol{A}$ is a $K \times K$ matrix, $\boldsymbol{b}$ is a K-dimensional column vector, and $\boldsymbol{c}$ is a K-dimensional row vector. Here we dropped subscripts that identify the decoder number in order to simplify the notation (e.g., $\boldsymbol{A}_i$ in the main text is simply expressed $\boldsymbol{A}$ here) because we are describing a general theory. It is known that the transfer function $\tilde{h}(s)$ of the linear system of Eq. (S21) is given by

$$\tilde{h}(s) = \boldsymbol{c}(s\boldsymbol{I} - \boldsymbol{A})^{-1}\boldsymbol{b} = \sum_{i=0}^{\infty} \frac{1}{s^{i+1}} \boldsymbol{c}\boldsymbol{A}^i\boldsymbol{b},$$

where $\boldsymbol{I}$ is the identity matrix. Since the transfer function depends only on $\boldsymbol{c}\boldsymbol{A}^i\boldsymbol{b}$, the transfer function is invariant under coordinate transform $\boldsymbol{z}' = \mathcal{T}\boldsymbol{z}$, where $\mathcal{T}$ is a regular matrix. According to the Faddeev method, $(s\boldsymbol{I} - \boldsymbol{A})^{-1}$ can be calculated by the following formula:

$$(s\boldsymbol{I} - \boldsymbol{A})^{-1} = \frac{\boldsymbol{F}_1 s^{K-1} + \cdots + \boldsymbol{F}_{K-1}s + \boldsymbol{F}_K}{s^K + f_1 s^{K-1} + \cdots + f_{K-1}s + f_K}, \tag{S22}$$

where $\boldsymbol{F}_i$ and f_i are defined as follows:

$$\boldsymbol{F}_1 = \boldsymbol{I}, \quad f_1 = -\mathrm{tr}\boldsymbol{A}, \quad \boldsymbol{F}_i = \boldsymbol{A}\boldsymbol{F}_{i-1} + f_{i-1}\boldsymbol{I}, \quad f_i = -\frac{1}{i}\mathrm{tr}(\boldsymbol{A}\boldsymbol{F}_i). \tag{S23}$$

We consider the following rational polynomial transfer function:

$$\tilde{h}(s) = \frac{\beta_1 s^{K-1} + \cdots + \beta_{K-1}s + \beta_K}{s^K + \alpha_1 s^{K-1} + \cdots + \alpha_{K-1}s + \alpha_K}, \tag{S24}$$

where α_i and β_i are real coefficients. One possible realization of the transfer function of Eq. (S24) in the form of Eq. (S21) is

$$\boldsymbol{A} = \begin{bmatrix} 0 & 0 & 0 & \cdots & -\alpha_K \\ 1 & 0 & 0 & \cdots & -\alpha_{K-1} \\ 0 & 1 & 0 & \cdots & -\alpha_{K-2} \\ \vdots & \vdots & \vdots & \ddots & \vdots \\ 0 & 0 & 0 & 1 & -\alpha_1 \end{bmatrix}, \quad \boldsymbol{b} = \begin{bmatrix} \beta_K \\ \beta_{K-1} \\ \beta_{K-2} \\ \vdots \\ \beta_1 \end{bmatrix}, \quad \boldsymbol{c} = [\ 0 \quad 0 \quad \cdots \quad 0 \quad 1\ ], \tag{S25}$$

which is known as the controller canonical form. Because of $\boldsymbol{c}$ in Eq. (S25), the output is given by the last variable $y(t) = z_K(t)$. The correctness of Eq. (S25) can be verified by calculating the transfer function through the Faddeev method [Eqs. (S22) and (S23)].

In the main text, we consider network realization for basis set A, whose basis functions are

$$\eta_1(t) = \sqrt{\frac{2}{3}}(1 - \cos(2\pi t)),$$
$$\eta_2(t) = \frac{2}{\sqrt{3}}\Theta\left(\frac{1}{2} - t\right)(1 - \cos(4\pi t)),$$

where $\Theta(t)$ is a step function. Since the step function yields a transfer function that does not fit into the form of Eq. (S24), we apply the Fourier series expansion to $\eta_2(t)$ to obtain

$$\eta_2(t) = \frac{16\sin(2\pi t)}{3\sqrt{3}\pi} - \frac{16\sin(6\pi t)}{15\sqrt{3}\pi} - \frac{\cos(4\pi t)}{\sqrt{3}} + \frac{1}{\sqrt{3}}.$$

In Fig. S1(c), we compare $\eta_2(t)$ for the exact function (solid line) and the Fourier approximation (dashed line). The Laplace transforms of $\eta_i(T-t)$ are given by

$$\tilde{\eta}_1(s) = \mathcal{L}[\eta_1(T-t)] = \sqrt{\frac{2}{3}}\frac{1}{s} - \sqrt{\frac{2}{3}}\frac{s}{s^2+4\pi^2},$$
$$\tilde{\eta}_1(s) = \mathcal{L}[\eta_2(T-t)] = -\frac{s}{\sqrt{3}\,(s^2+16\pi^2)} - \frac{32}{3\sqrt{3}\,(s^2+4\pi^2)} + \frac{32}{5\sqrt{3}\,(s^2+36\pi^2)} + \frac{1}{\sqrt{3}s},$$

where $\mathcal{L}$ is the Laplace transform operator. From Eq. (S16), the Laplace transform of optimal linear response function $h_i(t)$ (i.e., the transfer function) is

$$\tilde{h}_i(s) = \mathcal{L}[h_i(t)] = -\frac{1}{4\Lambda_i D_i}\sum_j \lambda_{ij}\tilde{\eta}_j(s).$$

Since Λ_i and λ_{ij} are real values, $\tilde{h}_i(s)$ fits into the form of Eq. (S24).

We next show explicit representations of $\boldsymbol{A}$ and $\boldsymbol{b}$ which are realizations of optimal linear response functions $h_i(t)$ ($h_1(t)$ and $h_2(t)$ in Fig. 3(a)). We use $\boldsymbol{A}_i$ and $\boldsymbol{b}_i$ to represent $\boldsymbol{A}$ and $\boldsymbol{b}$ of the ith decoder:

$$\boldsymbol{A}_1 = \begin{bmatrix} 0.0 & 0.0 & 0.0 & 0.0 & 0.0 & 0.0 & 0.0 \\ 10.0 & 0.0 & 0.0 & 0.0 & 0.0 & 0.0 & -22.15 \\ 0.0 & 10.0 & 0.0 & 0.0 & 0.0 & 0.0 & 0.0 \\ 0.0 & 0.0 & 10.0 & 0.0 & 0.0 & 0.0 & -76.37 \\ 0.0 & 0.0 & 0.0 & 10.0 & 0.0 & 0.0 & 0.0 \\ 0.0 & 0.0 & 0.0 & 0.0 & 10.0 & 0.0 & -55.27 \\ 0.0 & 0.0 & 0.0 & 0.0 & 0.0 & 10.0 & 0.0 \end{bmatrix}, \quad \boldsymbol{b}_1 = \begin{bmatrix} 3.78 \\ 1.50 \\ 2.32 \\ 1.13 \\ 0.35 \\ 0.11 \\ 0.0 \end{bmatrix}, \tag{S26}$$

$$\boldsymbol{A}_2 = \begin{bmatrix} 0.0 & 0.0 & 0.0 & 0.0 & 0.0 & 0.0 & 0.0 \\ 10.0 & 0.0 & 0.0 & 0.0 & 0.0 & 0.0 & -22.15 \\ 0.0 & 10.0 & 0.0 & 0.0 & 0.0 & 0.0 & 0.0 \\ 0.0 & 0.0 & 10.0 & 0.0 & 0.0 & 0.0 & -76.37 \\ 0.0 & 0.0 & 0.0 & 10.0 & 0.0 & 0.0 & 0.0 \\ 0.0 & 0.0 & 0.0 & 0.0 & 10.0 & 0.0 & -55.27 \\ 0.0 & 0.0 & 0.0 & 0.0 & 0.0 & 10.0 & 0.0 \end{bmatrix}, \quad \boldsymbol{b}_2 = \begin{bmatrix} 2.25 \\ -7.80 \\ 7.93 \\ -5.88 \\ 2.05 \\ -0.60 \\ 0.0 \end{bmatrix}. \tag{S27}$$

As denoted above, these realizations are not unique, as any coordinate transformation yields the same transfer function. Thus we applied some scaling matrix to adjust excessively large values in Eqs. (S26) and (S27), which seem to be biologically infeasible. Network representations of Eqs. (S26) and (S27) are shown in Figs. 4(a) and (b) in the main text, where positive and negative elements in $\boldsymbol{A}_i$ and $\boldsymbol{b}_i$ are described by activation (arrow) and inhibition (bar-headed line), respectively.